Int. J. Heat Mass Transfer. Vol. 34, No. 9, pp. 2361–2372, 1991
Printed in Great Britain

0017–9310/91 $3.00 + 0.00

Experimental study of laminar mixed convection in the entrance region of a horizontal semicircular duct

Q. M. LEI and A. C. TRUPP
Department of Mechanical Engineering, University of Manitoba, Winnipeg, Manitoba, Canada R3T 2N2

(*Received* 25 *July* 1990 *and in final form* 25 *October* 1990)

Abstract—Combined free and forced convection is experimentally investigated for laminar water flow in the entrance region of a horizontal semicircular duct. With uniform heat input axially, measurements are made of axial and circumferential wall temperature variations, together with pressure drops across the heated section, in order to study the effects of the buoyancy-induced secondary flow. For mean Reynolds numbers ranging from 400 to 1600, a factor of over two for friction factor increase and a factor of over four for heat transfer enhancement are found at high heating rates (mean Rayleigh numbers up to 4.6×10^8). Local and fully developed Nusselt numbers show substantial circumferential variations and increase with increasing heat flux level. Correlations are provided which disclose some key features of the laminar mixed convection regime.

INTRODUCTION

THE PRESENT paper describes an experimental investigation of laminar combined free and forced convective flow and heat transfer in a horizontal semicircular duct, the geometry of which is of particular interest for flows through multipassage tubes in the chemical and food processing industries. These mixed convection flows have been predominately studied for horizontal circular tubes [1, 2] and rectangular channels [3, 4] with various thermal boundary conditions. However, no similar work to the present study has been reported so far.

For horizontal laminar pipe flows, widely scattered experimental data have long been attributed to the influence of buoyant forces [5, 6]. The thermogravitational forces were known to generate counter-rotating vortices which are symmetrical about a vertical meridian plane [7]. Due to the superposition of the vortex type secondary flow on the streamwise main flow, experimental results exhibited substantial circumferential temperature variations. Even for a uniform heated stainless steel tube, a maximum temperature difference of 45°C between the top and bottom of the tube was reported by Hong *et al.* [8]. Similarly, secondary flows were found to be strong enough to cause the circumferential Nusselt number to differ by as much as a factor of four [9], with the maximum occurring at the bottom and the minimum at the top of an isothermal tube. Besides heat transfer enhancement, buoyancy effects were also observed to profoundly distort the streamwise velocity profile [10]. This resulted in markedly higher friction factors than the corresponding isothermal values [1, 11]. But, only a few investigators have obtained experimental pressure drop data subject to significant buoyancy effects.

For horizontal rectangular channels (including the limiting cases of parallel-plate channels), most studies were focused on the thermal entrance region and on the thermal instability due to buoyant forces (e.g. Gilpin *et al.* [12]). Ou *et al.* [13] used a 2% deviation of local Nusselt number from the value for pure forced convection as the criterion to estimate the onset of the secondary flow (or thermal instability). Osborne and Incropera [14] found that onset of the secondary flow was advanced with increasing Grashof number and with decreasing Reynolds number. As a result, a typical longitudinal Nusselt number distribution [4] would have the following pattern. The sharp decline in the immediate neighborhood of the entrance indicated the development of the thermal boundary layer. Beyond onset of free convection effects, the Nusselt number began to exceed the forced convection limit but the decline still continued. As the secondary flow grows to destabilize the boundary layer, the decline terminated and heat transfer enhancement was most pronounced thereafter. As the heating continued, the Nusselt number attained a maximum and then dropped again. The Nusselt number oscillations were also disclosed by the heat transfer measurements of Nakamura *et al.* [15] for triangular ducts and Imura *et al.* [16] for an isothermal flat plate. Incropera and Schutt [17] numerically predicted these trends. Following their work, Mahaney *et al.* [18] concluded that, under certain conditions, the oscillations were damped and yielded a fully developed Nusselt number that substantially exceeded the value for pure forced convection.

For a horizontal semicircular duct, the orientation of the duct cross section also affects the mixed convection flow and heat transfer. For example, buoyancy effects for the flat surface on top will be different

NOMENCLATURE

A_n	actual flow area
c_p	specific heat
D	duct inside diameter
D_h	hydraulic diameter
F	Darcy friction factor, $(dP/dZ)D_h/(2\rho\bar{W}^2)$
g	gravitational acceleration
Gr	modified Grashof number, $\beta g\rho^2 D_h^4 q''/\mu^2 k$
Gz	Graetz number, $(D_h\ Re\ Pr)/Z$
h	convection coefficient
(H1)	axially uniform wall heat flux with uniform peripheral wall temperature
(H2)	axially and peripherally uniform heat flux
k	fluid thermal conductivity
L	total heated length
$\dot{m}$	mass flow rate
Nu	Nusselt number, hD_h/k
Nu_{lm}	axial length–mean Nusselt number defined by equation (11)
P	pressure
Pe	Péclet number, $Re\ Pr$
Pr	Prandtl number, $\mu c_p/k$
q''	input surface heat flux
Ra	modified Rayleigh number, $Gr\ Pr$
Ra'	modified Rayleigh number based on the inside diameter D, $Ra(D_h/D)^4$
Re	Reynolds number, $\rho D_h\bar{W}/\mu$
T	temperature
$\bar{W}$	cross-sectional mean axial velocity
Z, z^*	axial coordinate, $z^* = Z/(D_h\ Re\ Pr) = 1/Gz$.

Greek symbols

β	coefficient of thermal expansion
μ	fluid dynamic viscosity
ρ	fluid density
σ	standard deviation.

Subscripts

0	isothermal or pure forced convection
a, b, c	thermocouple positions at a measuring station
cr	critical
dia	diabatic condition
fd	fully developed conditions
$H1$	(H1) boundary condition
$H2$	(H2) boundary condition
m	bulk mean or based on mean fluid temperature between inlet and outlet
M	mean fluid temperature in the fully developed region
max	maximum
th	average Nu value defined by equation (4)
w	duct wall
z	axially local.

Superscript

$\bar{}$	average value.

from the effects for the duct with the flat surface at the bottom or vertical. Numerical predictions of such effects in a horizontal semicircular duct with the flat surface at the bottom were performed by Nandakumar *et al.* [19]. They simulated an axially uniform heat flux with an infinite thermal conductivity of the duct in the peripheral direction. Under hydrodynamically and thermally fully developed conditions, they found dual solutions with a two- or four-vortex flow pattern which is akin to the bifurcation phenomenon in the Taylor problem. In the range of their Grashof number, for $Pr = 5$, maximum heat transfer enhancement achieved a factor of about three while the fully developed friction factor exceeded the corresponding isothermal value by about 25%. However, Law *et al.* [20] failed to obtain the four-cell solution for $Pr < 5$ for the case where the top curved surface was insulated while the bottom flat surface was heated. For this non-uniform heating, heat transfer enhancement was more significant, with a factor of over four for $Pr = 5$.

Not all aspects of the above described phenomenon and overall results could be confirmed in the present study due to experimental limitations. The present investigation was originally designed to examine buoyancy effects on the laminar water flow and heat transfer in the thermal entrance region of a horizontal semicircular duct. No particular attention was given to the verification of the vortex pattern phenomenon. Instead, it was planned to test the duct at various orientations including the orientation of Nandakumar *et al.* [19]. The first arbitrary choice of orientation was the flat surface on top and this is reported in the present paper. The duct was subjected to an axially uniform heat input after the flow was hydrodynamically fully developed. Specifically, the main purposes of the study were: (1) to measure the streamwise pressure drops with and without heating; (2) to measure local circumferential variations in wall temperatures (as evidence of buoyancy effects); (3) to obtain heat transfer data under various flow and heating rates. Additional objectives were to correlate flow and heat transfer results and to estimate and correlate the onset of the buoyancy flow.

EXPERIMENTAL APPARATUS

Duct geometry

Five semicircular ducts, each 2 m long, were carefully manufactured using type K copper pipes

(i.d. = 49.8 mm and o.d. = 54.0 mm) and brass plates (3.175 mm thick). To examine the correctness of the geometry, inner and outer diameters as well as radii at each duct end were measured to be within $\pm 1\%$ of corresponding nominal values. Volume tests by filling water at room temperature to the duct gave a maximum relative error of 2%. Each duct was straight and the duct twist angles were all within 1°.

Test facility

Experiments were carried out in the test facility shown in Fig. 1. The working fluid (distilled water) was circulated around the closed loop by a centrifugal pump with a filter and a bypass line. The upstream bulk mean temperature was measured as the fluid entered the horizontal section of 3.8 m for the development of hydrodynamics. Following the heated section, the downstream bulk mean temperature was measured after the mixing chamber. The water was then cooled in one or two double-pipe, counterflow heat exchangers using city water as a heat sink. Before the test fluid was returned to the accumulating tank, its flow rate was measured by variable area type flowmeters.

Heated section

The heated section was 4.7 m long, on which a thin layer of insulating varnish was sprayed and a thin dielectric tape was wrapped. Two parallel lines of electric resistance wires (Hoskin Copel), having a total resistance of 6.6 Ω, were then tightly wound around the duct with an equal spacing of 5 mm. Uniformity was tested by measuring the wire resistance for each 200 mm axial length ($\Omega\ \text{mm}^{-1}$). This resulted in a maximum non-uniformity error of 6% relative to its mean value. Next, the duct was coated using a high thermal conductivity and high temperature cement to firmly position the wiring and to uniformly distribute heat. Input power was regulated by a power variac and measured by a digital wattmeter. Pressure drop across the heated section was sensed through a diaphragm differential pressure transducer and averaged by an analog computer. Wall temperatures were detected at 19 axial stations, each employing three thermocouples (as shown in Fig. 1). An additional eight thermocouples were mounted on the duct wall just before and after the heating in order to estimate heat conduction losses along the duct ends. All test sections were finally covered by a 50 mm layer of fiberglass insulation to minimize external heat losses.

PROCEDURE AND DATA REDUCTION

After all measuring devices were calibrated, isothermal pressure drop runs were conducted at increasing Reynolds numbers to determine the critical Reynolds number, Re_{cr}, for laminar–turbulent transition. Subsequently, local Reynolds numbers in the heat transfer tests were controlled so as to be less than this Re_{cr} value. In this investigation, 92 different condition runs were completed for mean Reynolds numbers ranging from 400 to 1600, and for mean Rayleigh numbers ranging from 5.6×10^6 to 4.6×10^8.

For each test run, at least 5 h of operation were needed to keep the input conditions unchanged before a thermal equilibrium was established. Then, all readings of wall and bulk thermocouples, flowmeters, wattmeter, and pressure drops were recorded. Meanwhile, heat conduction losses through the insulation were measured by attaching a thermoelectric heat flux transducer on the insulation at a number of axial locations. To take into account heat conduction dissipation along the longitudinal duct wall, the measured axial gradients of wall temperatures at the beginning and the end of the heating were used to correct the upstream bulk temperature and the down-

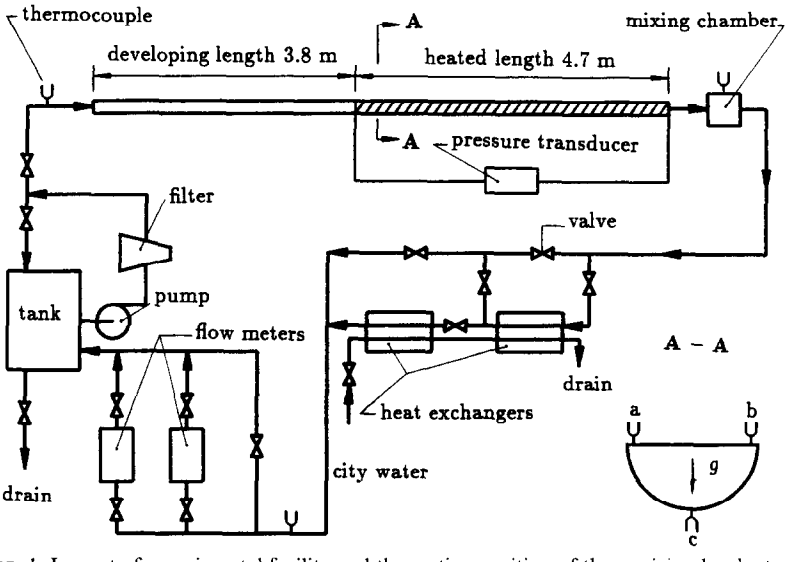

FIG. 1. Layout of experimental facility and the seating position of the semicircular duct.

stream bulk temperature. Between them, a straight line was fitted to determine local bulk temperatures. The rate of heat gain by the test fluid was then calculated and compared to the electric power input. Each set of data with an overall energy balance error within $\pm 8\%$ was accepted.

The Reynolds number and Darcy friction factor were defined, in terms of mass flow rate $\dot{m}$, pressure drop ΔP across the heated section L, and the actual flow area A_{fl}, as

$$Re = \frac{D_{\mathrm{h}}\dot{m}}{\mu A_{\mathrm{fl}}} \quad \text{and} \quad f = \frac{\Delta P D_{\mathrm{h}} \rho A_{\mathrm{fl}}^2}{2L\dot{m}^2}. \tag{1}$$

The modified Grashof number and Rayleigh number were defined by

$$Gr = \frac{\beta g \rho^2 D_{\mathrm{h}}^4 q''}{\mu^2 k} \quad \text{and} \quad Ra = Gr\,Pr. \tag{2}$$

Using the hydraulic diameter D_{h}, the local Nusselt number was also given by

$$Nu_{z,i} = \frac{h_{z,i} D_{\mathrm{h}}}{k} = \frac{q'' D_{\mathrm{h}}}{k(T_{z,i} - T_{z,\mathrm{m}})} \tag{3}$$

where i refers to a, b, and c for the wall thermocouple positions as shown in Fig. 1. The fluid thermal conductivity k was evaluated at the local bulk mean temperature $T_{z,\mathrm{m}}$. The local but peripherally averaged Nusselt numbers could be obtained either by averaging the peripheral wall temperatures $T_{z,i}$, or by averaging the peripheral heat transfer coefficients $h_{z,i}$. Due to symmetry, a better way to average a peripheral quantity ($T_{z,i}$ or $h_{z,i}$) may be, taking $\overline{T_{z,i}}$ as an example, like $\overline{T_{z,i}} = ((T_{z,\mathrm{a}} + T_{z,\mathrm{c}})/2 + (T_{z,\mathrm{b}} + T_{z,\mathrm{c}})/2)/2$. It is also useful to obtain the mean value of these two local average Nusselt numbers, denoted by $\overline{Nu}_{z,\mathrm{th}}$, which is given by

$$\overline{Nu}_{z,\mathrm{th}} = \left(\frac{\overline{h_{z,i}} D_{\mathrm{h}}}{k} + \frac{q'' D_{\mathrm{h}}}{k(\overline{T_{z,i}} - T_{z,\mathrm{m}})} \right) \Big/ 2. \tag{4}$$

Experimental uncertainties were estimated using the method of Holman [21]. For this experiment, friction factors and Reynolds numbers were considered to be accurate to within ± 8 and $\pm 4\%$, respectively. Regarding heat transfer, it is noted first that effects of axial heat conduction through the duct wall might cause the heat flux gained by the fluid to differ from the heat flux imposed on the outer surface of the duct. Such effects were significant in the thermal entrance region but they diminished as the change in the axial gradients of wall temperatures decreased. Assuming peripheral uniform conditions, an analysis [22] was performed which predicted a maximum difference of 3% between the fluid heat flux and the input flux on the outer surface of the duct. Including this consideration, uncertainties for the Rayleigh number and Nusselt number were estimated to be within ± 12 and $\pm 14\%$, respectively.

RESULTS AND DISCUSSION

Isothermal and diabatic friction factors

Figure 2 shows both the isothermal friction factor and a typical diabatic result. The f values for $Ra_{\mathrm{m}} = 0$, which are subjected to fully developed conditions, monotonically drop with increasing Re in the laminar region. These results are in good agreement with the Darcy friction factor prediction of $15.7668/Re$ [23, 24], with a maximum deviation of 8%. At the critical Reynolds number $Re_{\mathrm{cr}} \approx 2100$, a sudden jump in the value of f indicates the laminar–turbulent transition. For a heating case, as shown in Fig. 2 for $Ra_{\mathrm{m}} = 1.73 \times 10^8$, significant increases in f can be seen especially at low Re. These are due to buoyancy effects on axial velocity distributions. As Re decreases, the intensity of buoyancy-induced secondary flow becomes relatively stronger (e.g. having higher values of Gr/Re^2). This causes a more severe distortion of the axial velocity profile, hence resulting in large increases in the f values.

Buoyancy effects on friction factor are further illustrated in Fig. 3 which shows the ratio of diabatic friction factor (f_{dia}) to isothermal friction factor (f). Fluid properties are based on the average of the upstream bulk temperature and the downstream bulk temperature; this is indicated by the subscript m for Gr_{m} and Re_{m}. The augmentation can be observed to be as much as a factor of two at high Gr_{m}. As suggested in ref. [22], the Grashof number Gr_{m}, rather than the Rayleigh number Ra_{m}, was used to correlate the experimental data and a least-squares-fit expression is given by

$$\frac{(f_{\mathrm{dia}}\,Re)_{\mathrm{m}}}{(f\,Re)_{\mathrm{fd,0}}} = 1 + 5.269 \times 10^{-10} (Gr_{\mathrm{m}})^{1.138} \qquad (\sigma = 7.5\%, \sigma_{\max} = 16\%) \tag{5}$$

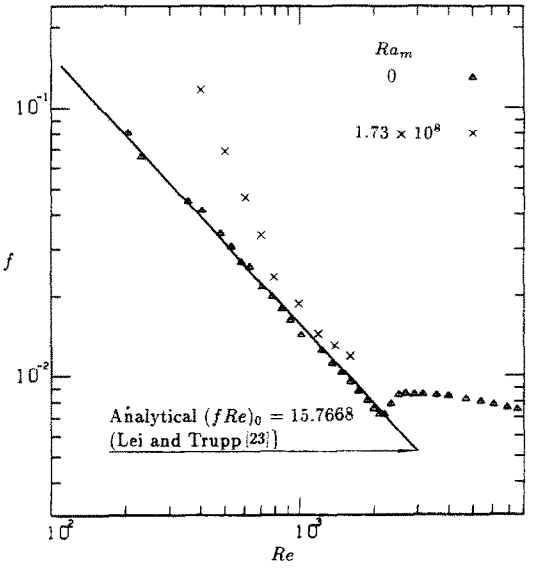

FIG. 2. f vs Re variation.

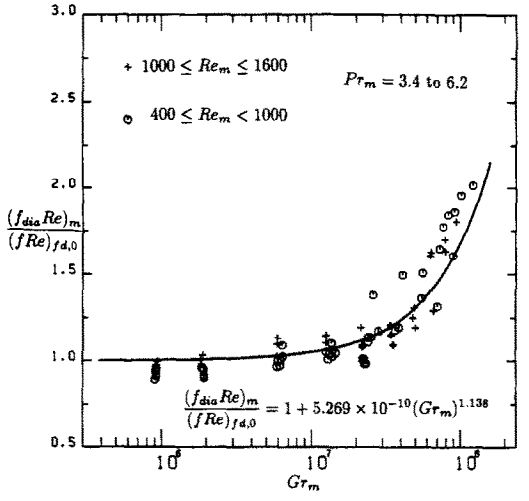

FIG. 3. Buoyancy effects on diabatic friction factor.

which satisfies the lower limit value of the ratio $(f_{dia}\ Re)_m/(f\ Re)_{fd,0}$. Equation (5) correlates all data fairly well, having a standard deviation (σ) of 7.5% over the average of the friction ratio in the range and a 16% maximum deviation (σ_{max}).

Note that in Fig. 3 all the data are divided into two groups partitioned at $Re_m = 1000$. An attempt to isolate the small Re_m effect on the friction ratio revealed the following pattern. For $Gr_m \leqslant 2 \times 10^7$, the ratios, which rise slightly with increasing Gr_m, show only a very weak dependence on Re_m. The data points for $Re_m < 1000$ appear somewhat lower than those for $Re_m > 1000$. Besides the experimental uncertainties, this is probably due mainly to fluid property variations (e.g. high flow rates bring about relatively low fluid axial temperature rises which tend to reduce the effect of fluid property variations, hence nearly giving an expected unit ratio at low Gr_m). On the other hand, for $Gr_m > 2 \times 10^7$, it is apparent that friction factor ratios increase markedly with increasing Gr_m. For a given Gr_m, the ratio is now generally somewhat higher for data with $Re_m < 1000$. This can probably be attributed to relative buoyancy effects, e.g. for low Re, a higher Gr/Re^2 value, as discussed earlier. Furthermore, by examining each cluster of measured points, most lower friction factor ratios in the cluster correspond to higher Prandtl numbers, e.g. as shown in Fig. 3 (by heavily bold symbols) for the data points for $Gr_m = 2 \times 10^7$–4×10^7 and $Pr > 5$. This is consistent with the Pr-dependence trend predicted by Nandakumar *et al.* [19].

It should be noted that, in the existing literature, no similar experimental data are available. A comparison was made (not illustrated) with the friction ratio of Morcos and Bergles [1] who studied laminar flow in a stainless steel tube using ethylene glycol as a working fluid. For a given value of Gr_m, their friction ratios were higher than the present results. This is also consistent with the predictions of Nandakumar *et al.* [19] who found that circular tubes resulted in higher friction ratios than semicircular ducts. However, direct comparison of the present friction factor ratios with their predictions are not appropriate. The first reason is that the pressure drop across the entire heated section is provided here while the friction factor only in the fully developed region was studied in ref. [19]. In addition, the duct orientation and the heating rate ranges for their study were different from the present investigation.

Wall temperature

Typical axial distributions of wall temperatures for two different heating rates are shown in Fig. 4. At each axial station, three temperatures are shown corresponding to the three thermocouples (see Fig. 1 for the positions). These provide an indication of peripheral variations in wall temperatures. As illustrated, all T_a values are nearly equal to T_b. This indicates that in the present study, a symmetric three-dimensional flow exists about the vertical center plane of the duct. However, all wall temperatures at the duct bottom, T_c, are noticeably lower than T_a or T_b, except for near the entrance where free convection effects are negligible. In this early thermal boundary layer development region, the copper duct distributes heat fairly uniformly on the circumferential walls of the duct. This is particularly evident for the lower heating rates in Fig. 4(a). Thus, the theoretical thermal boundary condition, (iii), which states uniform heat flux axially with uniform peripheral wall temperature, may be utilized as a good approximation.

As the thermal boundary layer develops, the heated fluid near the bottom becomes lighter and rises up while, by continuity, the cooler and heavier core fluid descends. As a result, the buoyancy-induced second-

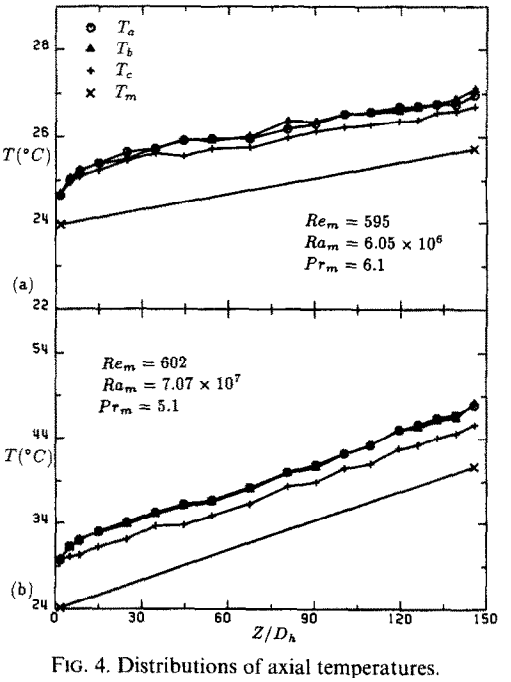

FIG. 4. Distributions of axial temperatures.

ary flow gives rise to the variation of circumferential wall temperatures. The first discernible reduction of T_c relative to T_a or T_b indicates the onset of the secondary flow. In Fig. 4(b), this reduction is observed to occur at a much earlier longitudinal station than for Fig. 4(a) where Ra_m is lower. This indicates earlier onset of the secondary flow with increasing Ra_m. Beyond that, the secondary flow continues to grow and causes T_c to remain relatively lower. It is then followed by fluctuations in the rising T_c due to the strengthening and weakening pattern (as discussed later) of thermal instability at the bottom surface. In contrast, the increase of T_a or T_b is more stable because of the thermal stratification of the top boundary layer. These results are consistent with the flow visualization and temperature measurements of Osborne and Incropera [14] who observed a weak buoyancy influence on their top plate condition for parallel plates with asymmetric heating.

Local heat transfer

Figure 5 illustrates typical Nusselt number distributions with the inverse Graetz number z^* for the same conditions as those in Fig. 4(a). At each location, Nusselt numbers for positions a and c as well as a cross-sectional-average value are presented. For $z^* < 0.001$, they nearly fall between the two forced convection limits of ref. [25] for the (H1) and (H2) conditions as defined in the Nomenclature. The expected decay in Nu_z and its small circumferential variation indicate that the dominant laminar forced convection flow still has negligible free convection effects. As z^* increases beyond about 0.001, temperature gradients at the bottom surface first induce thermal instability, resulting in a lower temperature at the surface (Fig. 4(a)) hence a higher $Nu_{z,c}$ value. With the development of the secondary flow, $Nu_{z,c}$ progressively exceeds its

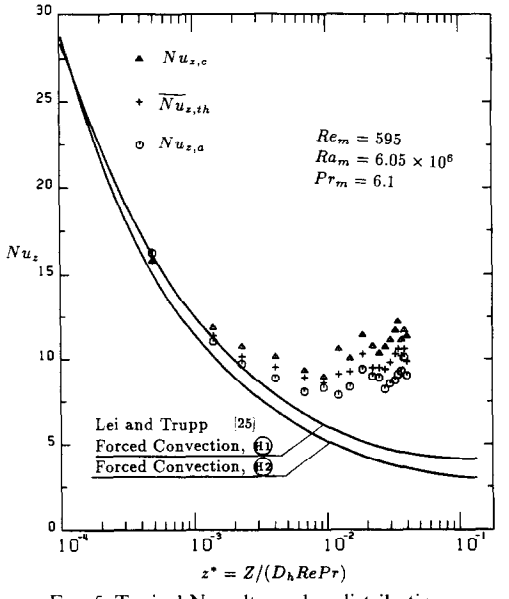

FIG. 5. Typical Nusselt number distributions.

forced convection limits and the difference between $Nu_{z,a}$ and $Nu_{z,c}$ becomes appreciable. At $z^* \approx 0.01$, a minimum for $\overline{Nu}_{z,th}$ is observed. Subsequently, $\overline{Nu}_{z,th}$ increases due to the increased importance of the secondary flow until its first maximum is reached at $z^* \approx 0.018$. The maximum is followed by a decreasing trend in all local Nusselt numbers. This is because the core fluid has already been warmed by the secondary flow and the reduction in the surface temperature by the descending fluid is less pronounced. Accordingly, the cross-sectional fluid circulation becomes weaker and the Nusselt numbers begin to decline. As the heating continues, the decline ends, e.g. at $z^* \approx 0.028$ for the second minimum of $\overline{Nu}_{z,th}$. Beyond the minimum point, the warm fluid rising and the cool fluid descending once more strengthens the secondary flow and causes another increase in the Nusselt number. Further observations suggest that the fully developed conditions for the mixed convection flow have been practically achieved within the last six stations. Although the continuing oscillations can still be seen in this fully developed region, especially for $Nu_{z,c}$, the magnitude between a peak and a valley is now relatively much less. In effect, the development of the secondary flow is first such that it 'overshoots' its steady-state strength, but it is forced to return since temperature differences (which drive the buoyancy forces) have been diminished. There is then an 'undershoot' in which temperature differences are regained to cause a subsequent correction.

As just described, the foregoing oscillations in Nusselt numbers have been recognized by many investigators. A recent numerical study on laminar mixed convection in the entrance region of a horizontal rectangular duct by Mahaney *et al.* [26] reported that the secondary flow is characterized by a fluctuating intensity along the longitudinal direction, which is consistent with the above observations. Since the secondary flow itself attenuates its size and strength and is intensified by further heating, the oscillating behavior should be detected in both measurements and predictions of horizontal laminar mixed convection flows.

Effect of Reynolds number

Comparisons of the local cross-sectional-average Nusselt number $\overline{Nu}_{z,th}$ for three different Re_m, but $Ra_m \approx 1.17 \times 10^7$, are made in Fig. 6 using the coordinates of Z/D_h and z^*. The effect of Reynolds number on $\overline{Nu}_{z,th}$ in Fig. 6(a) appears weak except for $Z/D_h \lesssim 25$. At the first station, $Z/D_h = 1.8$, fluid axial heat conduction appreciably influences $\overline{Nu}_{z,th}$, giving a lower $\overline{Nu}_{z,th}$ value for a smaller Péclet number ($Pe = Re\,Pr$) and a higher $\overline{Nu}_{z,th}$ value for a larger Pe. Such characteristics are consistent with those of pure forced convection laminar flow as documented in great detail by Shah and London [24]. In the presence of free convection effects, decreasing Reynolds number can be observed from Fig. 6(a) to shift the onset (defined later) of the secondary flow upstream (see

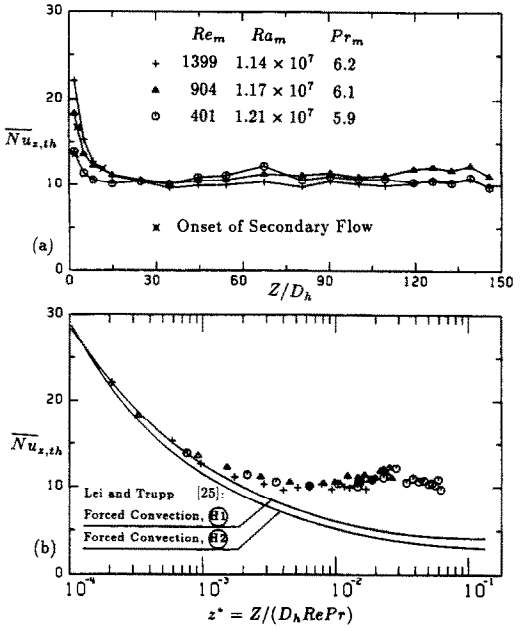

FIG. 6. Influence of Reynolds number on local Nusselt numbers for $Ra_m \approx 1.17 \times 10^7$.

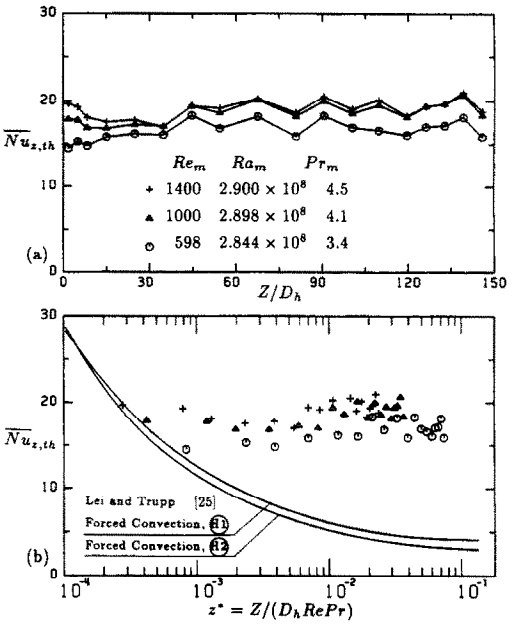

FIG. 7. Influence of Reynolds number on local Nusselt numbers for $Ra_m \approx 2.88 \times 10^8$.

the start symbol for the onset locations). Maughan and Incropera [4] have demonstrated a similar pattern in heat transfer measurements for airflow in a horizontal parallel plate channel. Other experimental results with $Ra_m < 7 \times 10^7$ [27] and numerical predictions [17, 28] suggest that mixed convection flows may be scaled with the inverse Graetz number, z^*. The present results are thus shown in Fig. 6(b) where $\overline{Nu}_{z,th}$ vs z^* is seen to be fairly independent of Re_m. Hence, at low or medium heating rates, Re_m, though stretching the flow, has practically little influence on the local Nusselt number when z^* is used as a scaling parameter.

The influence of Reynolds number on $\overline{Nu}_{z,th}$ is further shown in Fig. 7 for a higher Rayleigh number ($Ra_m \approx 2.88 \times 10^8$). At this much higher heating rate, the destabilization of the thermal boundary layer occurs further upstream. Reducing Reynolds number not only advances the onset of secondary flow but also decreases $\overline{Nu}_{z,th}$ (Fig. 7(a)), i.e. there appears to be a distinct Re_m dependence. In addition, the present results show considerable scatter when plotted against the inverse Graetz number (Fig. 7(b)) although experimental uncertainties and fluid property variations are considered to contribute partially to this scatter. With increasing Ra_m, the intensity of the secondary flow increases and hence may promote earlier transition to turbulent free convection. Existing experimental results of other investigators [11, 16, 29] also display substantial fluctuations with Reynolds number, particularly when subjected to high heating rates. Another possible reason for the Re_m dependence at high Ra_m may be accounted for by the type of vortex secondary flow pattern which has been explored by Nandakumar *et al.* [19] for fully developed laminar mixed convection flows.

Effect of Rayleigh number

A sample illustration of the Rayleigh number influence on $\overline{Nu}_{z,th}$ is provided in Fig. 8 for three different Ra_m but approximately the same Re_m. The zero Ra_m line for the (H1) condition serves well as a base-line reference for the lowest heating rate in the laminar forced convection region. First, increasing Ra_m can be

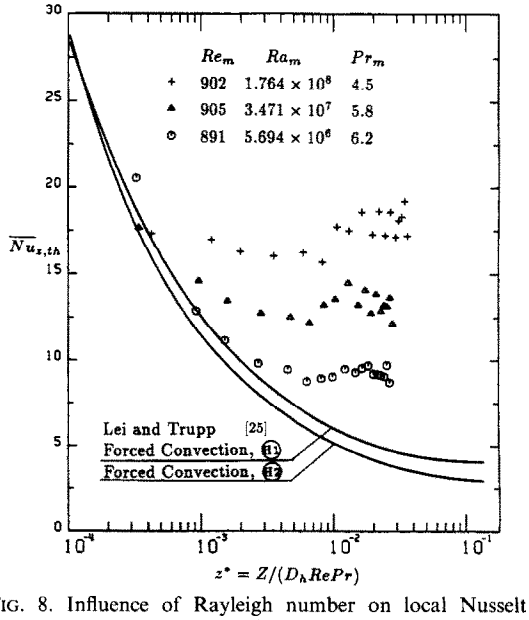

FIG. 8. Influence of Rayleigh number on local Nusselt numbers.

seen to have a strong effect on heat transfer enhancement. The fully developed results of $\overline{Nu}_{fd,th}$ for these three Ra_m exceed respectively a factor of 2.2, 3.2, and 4.4 over $(Nu_{fd,H1})_0$, and 3.1, 4.5, and 6.2 over $(Nu_{fd,H2})_0$, where $(Nu_{fd,H1})_0$ and $(Nu_{fd,H2})_0$ are the fully developed Nusselt numbers for the laminar forced convection flow [30, 31]. The enhancement is due to the presence of free convection currents which form a powerful mechanism for the fluid to transport momentum and thermal energy. Secondly, increasing Ra_m is observed to shorten the thermal entrance length and to move the onset of the secondary flow upstream. Thirdly, Fig. 8 shows that the frequency and magnitude of oscillations in $\overline{Nu}_{z,th}$ (as discussed before) decrease with reducing Ra_m or weakening of the secondary flow.

Onset of the secondary flow

The axial distance where the local $\overline{Nu}_{z,th}$ value first exceeds 5% of the forced convection value $(Nu_{z,H1})_0$ was taken to mark the onset of the secondary flow. From previous observations, the onset point was known to advance with reducing Reynolds number and with increasing Rayleigh number. This suggests that the critical value $(Z/D_h)_{cr}$ may be correlated with the parameter of $(Gr/Re^2)_{cr}$. Figure 9 indeed shows this to be the case. As illustrated, the majority of the data points for $(Z/D_h)_{cr}$ are below 5 which correspond to values over 3 for $(Gr/Re^2)_{cr}$. These indicate the early onset of the secondary flow for most test runs in which about 96% of the heated section (note, $L/D_h \approx 150$) was subjected to significant free convection effects. Such an expected outcome is due to the use of a relatively large hydraulic diameter ($D_h = 30.4$ mm) and high heat flux levels.

When studying the onset of the secondary flow in horizontal rectangular ducts, Ou *et al.* [13] correlated their Rayleigh number in terms of Graetz number while Gilpin *et al.* [12] correlated their Grashof number vs Reynolds number. Efforts to produce parallel correlations for the present experimental data were unsuccessful. However, as shown in Fig. 9, a least-squares fit gives the following expression:

$$\left(\frac{Z}{D_h}\right)_{cr} = 1.4 + 9.63\left(\frac{Gr}{Re^2}\right)_{cr}^{0.86} \quad (\sigma = 9\%,\ \sigma_{max} = 29\%) \quad (6)$$

which deliberately introduces a constant, 1.4, to better fit the majority of the data and correlates 83% of the data within 10%. Theoretically, $(Z/D_h)_{cr}$ should approach zero as $(Gr/Re^2)_{cr} \to \infty$ and vice versa. Clearly, equation (6) obeys the latter limit but approximates the former limit.

An empirical correlation obtained from Incropera *et al.* [32] for horizontal rectangular ducts is also illustrated in Fig. 9 (using $Pr = 5$ and $Re = 800$). Their onset points of the secondary flow, best fitted by $(Gr)_{cr} = 754(Gz)_{cr}^{4/3}$, were determined from measurement using a 10% enhancement of the Nusselt number. In spite of the different basis, as shown in Fig. 9 for $(Gr/Re^2)_{cr} > 20$, the present results indicate that the thermal boundary layer in the semicircular duct is more stable than that in a rectangular duct heated from below.

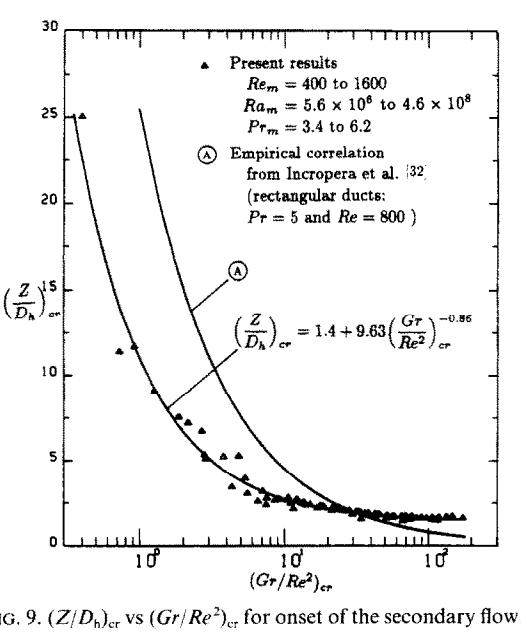

FIG. 9. $(Z/D_h)_{cr}$ vs $(Gr/Re^2)_{cr}$ for onset of the secondary flow.

Fully developed Nusselt number

Even though values of Nu_z (see Figs. 5–8) showed some buoyancy-induced fluctuations and fluid property variations in the flow direction, fully developed conditions were established in most test runs after the eighth wall-temperature-measuring station. To remove the influences of the above factors, values for the fully developed Nusselt number Nu_{fd} were determined by computing the length-mean average of Nu_z after the twelfth station. Similarly, other quantities (e.g. Re_M, Ra_M, Pr_M, and T_M, etc.) were obtained.

Figure 10 demonstrates effects of both Ra_M and Re_M on fully developed heat transfer results. $\overline{Nu}_{fd,th}$ was first normalized by the forced convection $(Nu_{fd,H1})_0$ value ($(Nu_{fd,H1})_0 = 4.088$ [30]). Then, it was multiplied by a viscosity ratio (as recommended by Kays and Crawford [33]) to take account of fluid property variations in the cross section. As can be seen, increasing Ra_M enhances heat transfer, with a factor up to 4.8 for high heating rates. On the other hand, within the experimental scatter, Re_M has little influence on heat transfer enhancement for $Ra_M \leqslant 5 \times 10^7$, which is in agreement with the previous observation made in connection with the thermal entrance region (see Fig. 6). But for higher Ra_M, the Nusselt ratios gradually increase with increasing Re_M. This trend, as discussed before, was revealed in Fig. 7 from the local Nusselt numbers. Such a Re_M dependence indicates that the experimental data might be correlated by the product of $Re_M\, Ra_M$ which has a

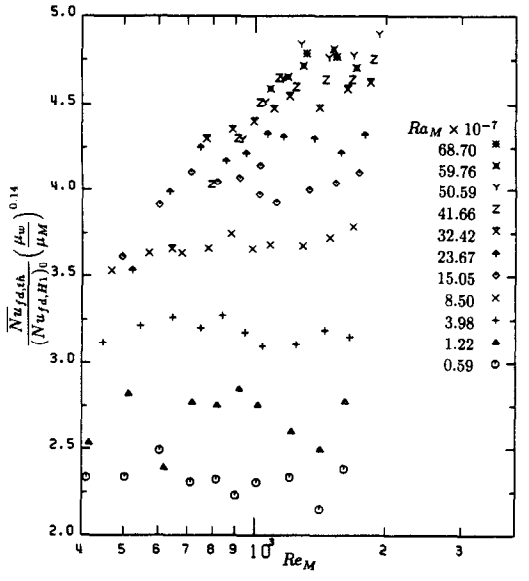

FIG. 10. Effects of Re_M and Ra_M on fully developed heat transfer enhancement.

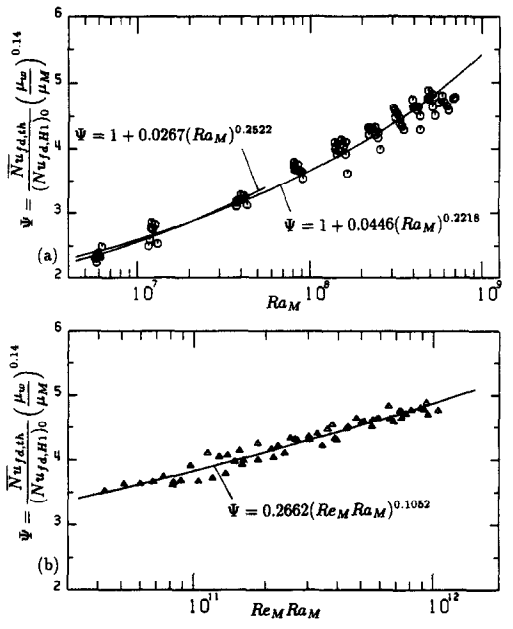

FIG. 11. Correlations of fully developed Nusselt ratios: (a) using Ra_M; (b) the Re_M-dependent data.

theoretical basis [34] and has been used successfully for circular tubes [35].

First, neglecting any Re_M dependence, the correlating equation can be expressed as

$$\frac{\overline{Nu}_{fd,th}}{(Nu_{fd,H1})_0} = 1 + 0.040(Ra_M)^{0.2288} \quad (\sigma = 4.6\%,\ \sigma_{max} = 9.2\%) \quad (7)$$

where unity is imposed to satisfy the low limit. By taking into account fluid property variation, an alternative correlation is given by

$$\frac{\overline{Nu}_{fd,th}}{(Nu_{fd,H1})_0}\left(\frac{\mu_w}{\mu_M}\right)^{0.14} = 1 + 0.0446(Ra_M)^{0.2218} \quad (\sigma = 4.0\%,\ \sigma_{max} = 8.8\%). \quad (8)$$

As indicated by the values of σ and σ_{max}, equation (8) fits the experimental data slightly better than equation (7). These two correlations are practically acceptable. Of course, as suggested by Fig. 10, still better correlations can be obtained by partitioning the data at $Ra_M = 5 \times 10^7$ into two sets. For $Ra_M < 5 \times 10^7$, the correlation is given by

$$\frac{\overline{Nu}_{fd,th}}{(Nu_{fd,H1})_0}\left(\frac{\mu_w}{\mu_M}\right)^{0.14} = 1 + 0.0267(Ra_M)^{0.2522} \quad (\sigma = 3.4\%,\ \sigma_{max} = 5.8\%). \quad (9)$$

This good correlation is illustrated in Fig. 11(a) together with equation (8). For $Ra_M > 5 \times 10^7$, the use of the $Re_M\,Ra_M$ product results in an excellent correlation which is given by

$$\frac{\overline{Nu}_{fd,th}}{(Nu_{fd,H1})_0}\left(\frac{\mu_w}{\mu_m}\right)^{0.14} = 0.2662(Re_M\,Ra_M)^{0.1052} \quad (\sigma = 2.3\%,\ \sigma_{max} = 4.7\%). \quad (10)$$

Figure 11(b) shows that the use of $Re_M\,Ra_M$ leads to Nusselt ratios being distributed very uniformly along the fitting curve.

Axial length–mean Nusselt number

For engineering purposes, information is also needed on average Nusselt values in the thermal entrance region. Figure 12 meets such demands by providing computed values for the axial length–mean Nusselt number, Nu_{lm}, which is defined by

$$Nu_{lm} = \frac{\int_0^L \overline{Nu}_{z,th}\,dZ}{L}. \quad (11)$$

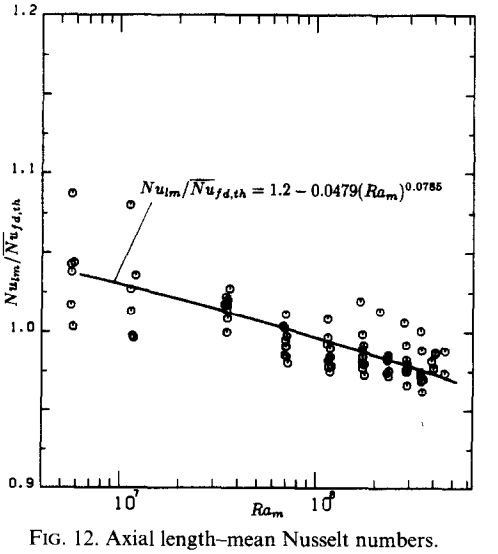

FIG. 12. Axial length–mean Nusselt numbers.

As illustrated, the $Nu_{lm}/\overline{Nu}_{fd,th}$ ratios range from 0.96 to 1.09. For $Ra_m < 7 \times 10^7$, most of the ratios are over 1. As Ra_m increases, the ratios are seen to decrease and most of the ratios become slightly less than 1. This is mainly due to the large values obtained for $\overline{Nu}_{fd,th}$ as buoyancy effects become increasingly significant. Also, note that for pure forced convection cases Nusselt numbers monotonically decrease with increasing axial length (e.g. in ref. [25]). The corresponding ratio of Nu_{lm} to the fully developed Nu value is known to be about 1.2. However, free convection effects generally cause the Nusselt number to vary nonmonotonically with the axial length. For example, referring to Fig. 8 for $Ra_M = 3.471 \times 10^7$, the axial Nusselt distribution first exhibits a marked decay for $z^* \leqslant 0.007$. The decay is then followed by significant increases in $\overline{Nu}_{z,th}$ as the secondary flow has a chance to be fully developed. Therefore, the shown 'valley' region is responsible for the 'undershoot' for Nu_{lm}, i.e. causing the $Nu_{lm}/\overline{Nu}_{fd,th}$ to be less than 1.

The data points shown in Fig. 12 also display some degree of fluctuation for a given Ra_m. Besides experimental uncertainties, this can be attributed to the Reynolds effect as discussed earlier. In any event, for design purposes, the average ratio for $Nu_{lm}/\overline{Nu}_{fd,th}$ is approximately unity, whereas the following correlation accurately describes the experimental data:

$$Nu_{lm}/\overline{Nu}_{fd,th} = 1.2 - 0.0479(Ra_m)^{0.0785} \quad (\sigma = 1.4\%,\ \sigma_{max} = 5\%). \quad (12)$$

Comparison of fully developed Nusselt numbers

Concerning fully developed heat transfer, Fig. 13 shows Nusselt number ratios vs Ra'_M (that is based on the inside diameter of the duct) which facilitates comparisons. Two comparisons are made in Fig. 13.

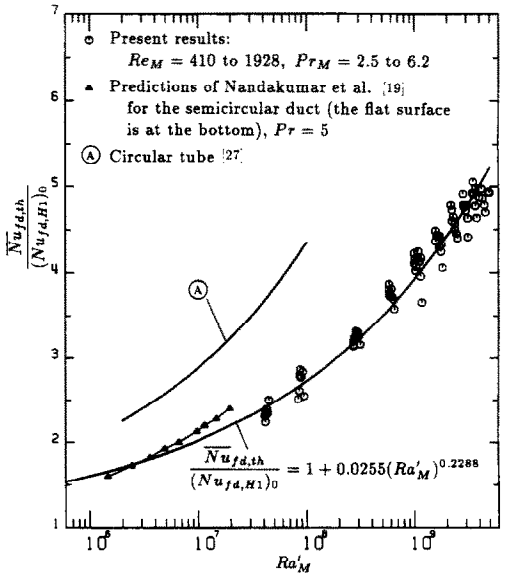

FIG. 13. Fully developed heat transfer enhancement and comparison with other results.

One is with the numerical results (two vortex) of Nandakumar *et al.* [19] for a semicircular duct with an axially uniform heat input. Note that under their fully developed conditions the duct seating position differs by 180° from the duct position in this investigation. Results obtained from equation (7) (converted to Ra'_M) agree well with the predicted values at low Ra'_M. This outcome suggests a weak effect of duct orientation on heat transfer enhancement at low Ra'_M. Of course, the duct orientation has no influence at all in the limiting case of zero buoyant force ($Ra'_M = 0$). As Ra'_M increases, the difference becomes appreciable, with about 10% deviation at $Ra'_M \approx 2 \times 10^7$. Although further studies on the duct orientation effects are required, the discrepancy shown is largely attributed to the difference between the theoretical condition (H1) and the practical resistance-wiring heating condition as well as fluid property variations. For high heating rates, large variations in circumferential wall temperatures were observed experimentally. Definitely, they are mainly induced by the secondary flow regardless of the high thermal conductivity of the copper duct. However, using the (H1) condition assumes a uniform peripheral wall temperature and hence cross-sectional temperature differences (e.g. $T_w - T_m$) or driving forces for the secondary flow are artificially much larger than the real situation. This is particularly true if the temperature differences near the duct bottom are concerned. Consequently, overpredictions might result.

Another comparison is provided in Fig. 13 with the empirical correlation of Rustum and Soliman [27] for a uniform heated smooth tube (here, $(Nu_{fd,H1})_0 = 4.36$). At $Ra'_M = 4.9 \times 10^6$, their correlation gives a Nusselt ratio which is about 1.4 times higher than that obtained from equation (7). At the same Rayleigh number, Nandakumar *et al.* [19] have numerically predicted that the Nusselt ratio for the circular tube is about 1.5 times higher than their semicircular duct. In addition, an earlier climb in the Nusselt ratio for a circular tube could be seen from Fig. 13 if all these curves were extrapolated back to very low Ra'_M. This indicates that the secondary flow in the semicircular duct begins to enhance heat transfer at a relatively larger Rayleigh number.

CONCLUSION

This experimental study was conducted on combined free and forced convection for laminar flow in a horizontal semicircular duct with uniform heat input axially. Results were limited to only one duct orientation (the flat wall on top) and the narrow range of Prandtl numbers for water. The main conclusions are as follows:

(1) Fully developed isothermal friction factors agree well with the theoretical prediction of $15.7668/Re$. Increases in the diabatic friction factor

are most pronounced in low Re_m and exceed a factor of 2 for high Gr_m.

(2) Since free convection effects are negligible very near the entrance, the experimental Nusselt numbers in this region generally fall between the two curves of pure forced convection for the (H1) and (H2) conditions. As the heating continues, buoyancy effects cause circumferential variations in wall temperatures and longitudinal oscillations in local Nusselt numbers.

(3) The Rayleigh number strongly influences heat transfer enhancement and advancement for onset of the secondary flow. Even though reducing Re_m can shift the onset point upstream, the heat transfer results are little affected by Re_m for $Ra_m < 5 \times 10^7$. But, for $Ra_m > 5 \times 10^7$, an Re_m dependence has been observed.

(4) Fully developed Nusselt numbers exceed a factor of four over the forced convection value ($(Nu_{fd,H1})_0 = 4.088$) at $Ra_M > 1.5 \times 10^8$. These results are well correlated by equations (7)–(10).

Acknowledgment—This research was supported by the Natural Sciences and Engineering Research Council of Canada.

REFERENCES

1. S. M. Morcos and A. E. Bergles, Experimental investigation of combined forced and free laminar convection in horizontal tubes, *ASME J. Heat Transfer* **97,** 212–219 (1975).
2. S. V. Patankar, S. Ramadhyani and E. M. Sparrow, Effect of circumferentially nonuniform heating on laminar combined convection in a horizontal tube, *ASME J. Heat Transfer* **100,** 63–70 (1978).
3. H. Nakamura, A. Matsuura and J. Kiwaki, Experimental study on heat transfer of combined free and forced laminar convection in thermal entrance region of horizontal rectangular ducts, *J. Chem. Engng Japan* **11,** 438–443 (1978).
4. J. R. Maughan and F. P. Incropera, Experiments on mixed convection heat transfer for airflow in a horizontal and inclined channel, *Int. J. Heat Mass Transfer* **30,** 1307–1318 (1987).
5. A. J. Ede, The heat transfer coefficient for flow in a pipe, *Int. J. Heat Mass Transfer* **4,** 105–110 (1961).
6. B. S. Petukhov and A. F. Polyakov, Flow and heat transfer in horizontal tubes under combined effect of forced and free convection, *Heat Transfer 1970, The 4th Int. Heat Transfer Conf.*, Vol. 4 (1970).
7. Y. Mori and K. Futagami, Forced convection heat transfer in uniformly heated horizontal tubes (2nd Report, theoretical study), *Int. J. Heat Mass Transfer* **10,** 1801–1813 (1967).
8. S. W. Hong, S. M. Morcos and A. E. Bergles, Analytical and experimental results for combined forced and free laminar convection in horizontal tubes, *Heat Transfer 1974, The 5th Int. Heat Transfer Conf.*, Vol. 3 (1974).
9. W. W. Yousef and J. D. Tarasuk, An interferometric study of combined free and forced convection in a horizontal isothermal tube, *ASME J. Heat Transfer* **103,** 249–256 (1981).
10. Y. Mori, K. Futagami, S. Tokuda and M. Nakamura, Forced convective heat transfer in uniformly heated horizontal tubes, *Int. J. Heat Mass Transfer* **9,** 453–463 (1966).
11. M. A. El-Hawary, Effect of combined free and forced convection on the stability of flow in a horizontal tube, *ASME J. Heat Transfer* **102,** 273–278 (1980).
12. R. R. Gilpin, H. Imura and K. C. Cheng, Experiments on the onset of longitudinal vortices in horizontal Blasius flow heated from below, *ASME J. Heat Transfer* **100,** 71–77 (1978).
13. J. W. Ou, K. C. Cheng and R. C. Lin, Natural convection effects on Graetz problem in horizontal rectangular channels with uniform wall temperature for large *Pr*, *Int. J. Heat Mass Transfer* **17,** 835–843 (1974).
14. D. G. Osborne and F. P. Incropera, Laminar, mixed convection heat transfer flow between horizontal parallel plates with asymmetric heating, *Int. J. Heat Mass Transfer* **28,** 207–217 (1985).
15. H. Nakamura, A. Matsuura and J. Kiwaki, Combined free and forced laminar convection in thermal entrance region of horizontal triangular ducts, *J. Chem. Engng Japan* **13,** 110–116 (1980).
16. H. Imura, R. R. Gilpin and K. C. Cheng, An experimental investigation of heat transfer and buoyancy induced transition from laminar forced convection to turbulent free convection over a horizontal isothermally heated plate, *ASME J. Heat Transfer* **100,** 429–434 (1978).
17. F. P. Incropera and J. A. Schutt, Numerical simulation of laminar mixed convection in the entrance region of horizontal rectangular ducts, *Numer. Heat Transfer* **8,** 707–729 (1985).
18. H. V. Mahaney, F. P. Incropera and S. Ramadhyani, Development of laminar mixed convection flow in a horizontal rectangular duct with uniform bottom heating, *Numer. Heat Transfer* **12,** 137–155 (1987).
19. K. Nandakumar, J. H. Masliyah and Hin-Sum Law, Bifurcation in steady laminar mixed convection flow in horizontal ducts, *J. Fluid Mech.* **152,** 145–161 (1985).
20. Hin-Sum Law, J. H. Masliyah and K. Nandakumar, Effect of nonuniform heating on laminar mixed convection in ducts, *ASME J. Heat Transfer* **109,** 131–137 (1987).
21. J. P. Holman, *Experimental Methods for Engineers*. McGraw-Hill, New York (1978).
22. Q. M. Lei, Numerical and experimental study of laminar mixed convection in a horizontal semicircular duct, Ph.D. Thesis, University of Manitoba, Winnipeg, Canada (1990).
23. Q. M. Lei and A. C. Trupp, Maximum velocity location and pressure drop of fully developed laminar flow in circular sector ducts, *ASME J. Heat Transfer* **111,** 1085–1087 (1989).
24. R. K. Shah and A. L. London, Laminar flow forced convection in ducts. In Supplement 1 to *Advances in Heat Transfer*. Academic Press, New York (1978).
25. Q. M. Lei and A. C. Trupp, Forced convection of thermally developing laminar flow in circular sector ducts, *Int. J. Heat Mass Transfer* **33,** 1675–1683 (1990).
26. H. V. Mahaney, F. P. Incropera and S. Ramadhyani, Effect of wall heat flux distribution on laminar mixed convection in the entrance region of a horizontal rectangular duct, *Numer. Heat Transfer* **13,** 427–450 (1988).
27. I. M. Rustum and H. M. Soliman, Experimental investigation of laminar mixed convection in tubes with longitudinal internal fins, *ASME J. Heat Transfer* **110,** 366–372 (1988).
28. G. J. Hwang and K. C. Cheng, Convective instability in the thermal entrance region of a horizontal parallel plate channel heated from below, *ASME J. Heat Transfer* **95,** 72–77 (1973).
29. A. L. Knox and F. P. Incropera, Mixed convection flow and heat transfer in the entry region of a horizontal rectangular duct, Paper 86-HT-18, AIAA/ASME Thermophysics and Heat Transfer Conf., Boston, Massachusetts (1986).
30. Q. M. Lei and A. C. Trupp, Further analyses of laminar flow heat transfer in circular sector ducts, *ASME J. Heat Transfer* **111,** 1088–1090 (1989).
31. A. C. Trupp and Q. M. Lei, Laminar flow heat transfer in circular sector ducts with uniform heat flux, *Trans. CSME* **13,** 31–34 (1989).

32. F. P. Incropera, A. L. Knox and J. A. Schutt, Onset of thermally driven secondary flow in horizontal rectangular ducts, *Proc. 8th Int. Heat Transfer Conf.*, San Francisco, Vol. 3, pp. 1395–1400 (1986).
33. W. M. Kays and M. E. Crawford, *Convective Heat and Mass Transfer*. McGraw-Hill, New York (1980).
34. B. R. Morton, Laminar convection in uniformly heated horizontal pipes at low Rayleigh numbers, *Q. J. Mech. Appl. Math.* **12**, 410–420 (1959).
35. S. Kakac, R. K. Shah and W. Aung, *Handbook of Single-phase Convective Heat Transfer*, Chap. 15. Wiley, New York (1987).

ETUDE EXPERIMENTALE DE LA CONVECTION MIXTE LAMINAIRE DANS LA REGION D'ENTREE D'UN TUBE HORIZONTAL SEMI-CIRCULAIRE

Résumé—La convection mixte naturelle et forcée est étudiée expérimentalement pour un écoulement d'eau laminaire dans la région d'entrée d'un conduit horizontal semi-circulaire. Avec une puissance thermique uniforme axialement, on mesure les variations axiale et circonférentielle de la température pariétale et de la perte de pression à travers la section chauffée, de façon à étudier les effets de l'écoulement secondaire induit par le flottement. Pour des nombres de Reynolds moyens entre 400 et 1600, le coefficient de frottement s'accroît d'un facteur deux tandis que le transfert de chaleur augmente d'un facteur quatre aux très grands régimes de chauffage (nombre de Rayleigh moyen atteignant $4{,}6 \times 10^5$). Les nombres de Nusselt locaux et pleinement établis montrent des variations circonférentielles marquées et ils augmentent avec le niveau du flux thermique. Des formules sont proposées qui conviennent au régime laminaire de convection mixte.

EXPERIMENTELLE UNTERSUCHUNG DER LAMINAREN MISCHKONVEKTION IM EINTRITTSBEREICH EINES HORIZONTALEN HALBKREISFÖRMIGEN KANALS

Zusammenfassung—Es wird die gemischte freie und erzwungene Konvektion für eine laminare Wasserströmung im Eintrittsbereich eines waagerechten halbkreisförmigen Kanals untersucht. Bei gleichbleibendem axialem Wärmeeintrag wird die Verteilung der Wandtemperatur in axialer und in Umfangsrichtung zusammen mit dem Druckverlust entlang der beheizten Sektion gemessen. Damit soll der Einfluß der auftriebsinduzierten Sekundärströmung ermittelt werden. Für mittlere Reynolds-Zahlen im Bereich von 400 bis 1600 und hohen Rayleigh-Zahlen (bis zu $4{,}6 \times 10^8$) wird eine Verdoppelung des Druckabfalls und eine Steigerung des Wärmetransports auf über das Vierfache festgestellt. Die örtliche Nusselt-Zahl und die Nusselt-Zahl bei voll ausgebildeter Strömung zeigen erhebliche Unterschiede am Umfang und steigen mit wachsendem Wärmestrom an. Es werden Korrelationen zur Beschreibung einiger Hauptgesichtspunkte der laminaren Mischkonvektion vorgeschlagen.

ЭКСПЕРИМЕНТАЛЬНОЕ ИССЛЕДОВАНИЕ ЛАМИНАРНОЙ СМЕШАННОЙ КОНВЕКЦИИ ВО ВХОДНОЙ ОБЛАСТИ ГОРИЗОНТАЛЬНОГО КАНАЛА ПОЛУКРУГЛОГО СЕЧЕНИЯ

Аннотация—Экспериментально исследуется смешанная свободная и вынужденная конвекция при ламинарном течении воды во входной области горизонтального канала полукруглого сечения. С целью изучения эффектов вторичного течения, вызванного подъемной силой, определяются изменения температур жидкости и стенки, а также перепада давления на нагреваемом участке в условиях постоянного аксиального подвода тепла. При средних числах Рейнольдса, изменяющихся от 400 до 1600, и высоких скоростях нагрева (средние числа Рэлея составляют до $4{,}6 \times 10^8$) наблюдается увеличение коэффициента трения более чем вдвое и интенсификация теплопереноса в четыре с лишним раза. Числа Нуссельта (как локальные, так и для развитого течения) претерпевают значительные изменения по окружности и увеличиваются с ростом теплового потока. Приводятся соотношения, характеризующие основные особенности режима ламинарной смешанной конвекции.